Compositionally Tunable Ternary $Bi_2(Se_{1-x}Te_x)_3$ and $(Bi_{1-y}Sb_y)_2Te_3$ Thin Films via Low Pressure Chemical Vapor Deposition

Sophie L. Benjamin[a,b], C. H. (Kees) de Groot[c], Chitra Gurnani[a,d], Samantha L. Hawken[a], Andrew L. Hector[a], Ruomeng Huang[c], Marek Jura[e], William Levason[a], Eleanor Reid[a], Gillian Reid[a*], Stephen P. Richards[a], Gavin B. G. Stenning[e]

Abstract

The synthesis and characterization of a series of chemically compatible chemical vapor deposition precursors, $[MCl_3(E^nBu_2)_3]$ (M = Sb or Bi; E = Se or Te), is described. These distorted octahedral complexes have been shown to function as single source precursors to deposit the corresponding phase pure binary M_2E_3 as thin films. The morphologies, compositions and structures of the resulting films have been examined in detail. Their resistivities, mobilities and carrier concentrations were also determined by Hall effect measurements. Nuclear magnetic resonance studies confirm that combining the kinetically labile $[BiCl_3(Se^nBu_2)_3]$ and $[BiCl_3(Te^nBu_2)_3]$ complexes in solution results in scrambling of the Se^nBu_2 and Te^nBu_2 ligands. Taking advantage of this, using the resultant mixtures of the precursors in various ratios leads to deposition of the ternary $Bi_2(Se_{1-x}Te_x)_3$ thin films onto SiO_2, allowing the Se:Te ratio to be varied across the full range of solid solution compositions. In a similar way, thin films of the ternary $(Bi_{1-y}Sb_y)_2Te_3$ phase are obtained from various ratios of the $[BiCl_3(Te^nBu_2)_3]$ and $[SbCl_3(Te^nBu_2)_3]$ precursors; in this case compositional variation as a function of deposition temperature is demonstrated. The ternary films are phase pure and their lattice parameters follow a Vegard's law trend, suggesting well distributed solid solutions.

Introduction

Antimony and bismuth chalcogenides, M_2E_3 (M = Sb, Bi; E = Se, Te) are layered semiconducting materials with narrow bandgaps; Bi_2Se_3 (0.24 eV), Bi_2Te_3 (0.16 eV) and Sb_2Te_3 (0.28 eV).[1,2] Their highly anisotropic hexagonal structures give rise to a number of interesting properties. The M_2E_3 semiconductors are of particular interest as thermoelectric materials for near room temperature applications. Bi_2Te_3 behaves as an n-type semiconductor, whilst Sb_2Te_3 is typically a p-type semiconductor, thus these materials may be used to produce thermoelectric generators in which the p- and n-type elements are coupled electrically in series and thermally in parallel.[3,4,5,6] Thermoelectric materials typically require high electrical conductivities, whilst

[a] Chemistry, University of Southampton, Southampton SO17 1BJ, U.K. Email: G.Reid@soton.ac.uk
[b] School of Science and Technology, Nottingham Trent University, Nottingham NG11 8NS, U.K.
[c] Electronics and Computer Science, University of Southampton, Southampton SO17 1BJ, U.K.
[d] School of Natural Sciences, Mahindra Ecole Centrale, Hyderabad, India.
[e] ISIS Neutron and Muon Source, Rutherford Appleton Laboratory, Harwell Science and Innovation Campus, Didcot, OX11 0QX, UK.

being thermally insulating. Electrical conductivities (σ) for the layered hexagonal materials, Bi_2Se_3 and Bi_2Te_3 produced from a range of deposition methods have been reported as 101–549 S cm^{-1} [7] and 312–8620 S cm^{-1}, respectively,[8,9,10,11,12] with values of 104–1695 S cm^{-1} for Sb_2Te_3.[9,13,14,15] Sb_2Se_3, on the other hand, adopts an orthorhombic structure and with its comparatively larger band gap (1.1 eV),[1] has intrinsically low electrical conductivity (10^{-6} to 10^{-7} S cm^{-1}).[16] Its high absorption coefficient (> 10^5 cm^{-1})[17] and dielectric constant of 29-18 within a 2 KHz to 2 MHz frequency range[18] bring interest for photovoltaic applications.[19,20] These materials are also topological insulators[21,22] and candidates for spintronic devices.[23]

Chemical vapor deposition (CVD) is widely employed for thin film deposition as it is a scalable and relatively inexpensive processing method.[24] A number of CVD approaches have previously been employed for M_2E_3 film growth, mostly using multi-source precursors. For example, Bi_2Se_3 has been deposited using $BiMe_3$ and $SeEt_2$ with H_2 carrier gas,[7] Bi_2Te_3 from $BiMe_3$ and Te^iPr_2,[8] and Sb_2Te_3 from SbR_3 (R = Me, Et) and TeR_2 (R = Et, ^{i}Pr).[25,26] However, single source precursors, in which both the metal and chalcogen are contained in a single molecule, can offer advantages, including increasing control of the stoichiometry of the resulting film, more efficient use of the precursor, as well as the use of easier-to-handle precursors (less hydrolytically sensitive and/or less pyrophoric). A small number of single source precursors for CVD of M_2E_3 have been reported, including $Bi[(SePR_2)_2N]_3$ (E = Se; R = Ph, ^{i}Pr),[27,28] whilst $[Sb\{(TeP^iPr_2)_2N\}_3]$ [29] and $[Sb\{SeC_5H_3(Me\text{-}3)N\}_3]$ [30] have been used to deposit Sb_2Te_3 under aerosol assisted (AA)CVD conditions and $[MeSb(E^nBu_2)_2]$ (E = Se, Te) can be used to deposit Sb_2Se_3 and Sb_2Te_3 thin films (the latter showing high selectivity for film growth onto TiN over SiO_2 on lithographically patterned substrates) under low pressure (LP)CVD conditions.[13,31] We have also reported single source precursors based upon molecular complexes of early transition metal and main group chlorides with neutral chalcogenoether ligands that are suitable for use in LPCVD for binary metal chalcogenide thin films.[32,33,34,35] The possibility of selective deposition of oriented thin films onto specific regions of lithographically patterned substrates has been realized using this family of precursors, including for $[BiCl_3(Te^nBu_2)_3]$.[12] This selectivity is atypical for CVD processing, which tends to lead to conformal coating of substrates. However, it could bring significant advantages in device fabrication, since, if the chalcogenide material can be deposited only onto pre-defined regions of patterned substrates, this would reduce the number of processing steps required (e.g. removing the need for unnecessary etching steps), as well as reducing the volume of the chalcogenide material required.

Whilst thermoelectric devices based upon n-type Bi_2Te_3 and p-type Sb_2Te_3 are available, significantly enhanced thermoelectric properties have been reported for ternary phases and superlattices of Bi_2Te_3 and Sb_2Te_3.[36,37] The ability to control the composition of thin films of the ternary materials is therefore of considerable interest to allow optimization of their properties for various applications.[38,39,40,41,42] For n-type Bi_2Te_3, one way of achieving this is to introduce selenium into the alloy, forming a solid solution of $Bi_2(Se_{1-x}Te_x)_3$, whilst optimization of p-type Sb_2Te_3 can be achieved by incorporation of bismuth, in $(Bi_{1-y}Sb_y)_2Te_3$. CVD routes that provide compositional control of these ternary materials as thin films are not well developed.

In this work we report the new reagents, $[BiCl_3(^nBu_2Se)_3]$, $[SbCl_3(Se^nBu_2)_3]$ and $[SbCl_3(^nBu_2Te)_3]$, and demonstrate their utility as single source precursors for the corresponding binary Bi_2Se_3, Sb_2Se_3 and Sb_2Te_3 films, respectively. We also demonstrate that by combining the appropriate, chemically compatible molecular precursors from across this homologous series (in combination with $[BiCl_3(Te^nBu_2)_3]$), it is possible to achieve compositional control within the thin films across the two ternary $Bi_2(Se_{1-x}Te_x)_3$ and $(Bi_{1-y}Sb_y)_2Te_3$ phases.

Experimental Section

Precursor synthesis

All precursor complexes were prepared using Schlenk, vacuum line and glove box techniques under a dry nitrogen atmosphere. The reagents were stored and manipulated using a dry, N_2-purged glove box. Hexane was dried by distillation over a sodium wire. Se^nBu_2,[43] Te^nBu_2[44] and $[BiCl_3(Te^nBu_2)_3]$[12] were prepared according to the literature methods. IR spectra were recorded as Nujol mulls between CsI plates using a Perkin-Elmer Spectrum 100 instrument. ^1H and $^{13}C\{^1H\}$ NMR spectra were recorded from solutions in $CDCl_3$ or CD_2Cl_2 on a Bruker AV400 spectrometer, $^{77}Se\{^1H\}$ and $^{125}Te\{^1H\}$ NMR spectra on a Bruker AV400 II spectrometer and referenced to external neat $SeMe_2$ and $TeMe_2$, respectively. Microanalytical results were obtained from Medac Ltd.

$[BiCl_3(Se^nBu_2)_3]$: $BiCl_3$ (0.10 g, 0.32 mmol) was dissolved in anhydrous MeCN (10 mL) and the solution cooled to 0 °C. A solution of Se^nBu_2 (0.18 g, 0.96 mmol) in MeCN (10 mL) was slowly added, giving a pale yellow solution which was allowed to warm to room temperature and then stirred for 1 h. The volatile components were removed *in vacuo*, leaving viscous yellow oil which was dried *in vacuo* for 1 h. Yield: 0.19 g, 68 %. ^1H NMR ($CDCl_3$): δ = 0.95 (*t*, [3H], CH_3), 1.46 (*m*, [2H], CH_2), 1.72 (*q*, [2H], CH_2), 2.99 (*t*, [2H], CH_2Se). $^{13}C\{^1H\}$ NMR ($CDCl_3$): δ = 13.6 (CH_3), 23.0 (CH_2), 27.2 (CH_2), 32.6 (CH_2Se). $^{77}Se\{^1H\}$ NMR ($CH_2Cl_2/CDCl_3$): δ = 184. IR (neat thin film /cm^{-1}): *v* = 267 br (Bi−Cl). Anal. calcd for $C_{24}H_{54}BiCl_3Se_3$: C 32.2, H 6.1; found: C 31.9, H 6.2%.

$[SbCl_3(Se^nBu)_3]$: Freshly sublimed $SbCl_3$ (0.228 g, 1.0 mmol) was dissolved in anhydrous MeCN (10 mL) and the solution cooled to 0 °C. A solution of Se^nBu_2 (0.580 g, 3.0 mmol) in MeCN (10 mL) was slowly added, giving a pale yellow solution which was allowed to warm to room temperature and then stirred for 1 h. The volatile components were removed *in vacuo*, leaving a pale yellow oil which was dried gently *in vacuo*. ^1H NMR ($CDCl_3$): δ = 0.91 (*t*, [3H], CH_3), 1.39 (*m*, [2H], CH_2), 1.63 (*q*, [2H], CH_2), 2.54 (*t*, [2H], CH_2Se). $^{13}C\{^1H\}$ NMR ($CDCl_3$): δ = 13.9 (CH_3), 23.6 (CH_2), 24.4 (CH_2), 33.3 (CH_2Se). $^{77}Se\{^1H\}$ NMR (CH_2Cl_2): δ = 168. IR (thin film/cm^{-1}): *v* = 306 br (Sb−Cl). Anal. calcd for $C_{24}H_{54}SbCl_3Se_3$: C 35.69, H 6.74; found: C 34.54, H 7.25%.

$[SbCl_3(Te^nBu_2)_3]$: $SbCl_3$ (0.228 g, 1.0 mmol) was directly reacted with Te^nBu_2 (0.725 g, 3.0 mmol) at room temperature, giving a dark orange/red oil; volatiles were removed . Yield: 0.19 g, 68%. ^1H NMR ($CDCl_3$): δ = 0.92 (*t*, [3H], CH_3), 1.41 (*m*, [2H], CH_2), 1.71 (*q*, [2H], CH_2), 2.72 (*t*, [2H], CH_2Te). $^{13}C\{^1H\}$ NMR ($CDCl_3$): δ = 4.28

(CH_2Te), 13.5 (CH_3), 25.8 (CH_2), 34.9 (CH_2). $^{125}Te\{^1H\}$ NMR (CH_2Cl_2): δ = 237. IR (neat thin film /cm^{-1}): *v* = 248 br (Sb−Cl). Anal. calcd for $C_{24}H_{54}SbCl_3Te_3$: C 30.2, H 5.7; found: C 29.9, H 5.7%.

Ternary precursors: NMR experiments

Samples of $[BiCl_3(Se^nBu_2)_3]$ and $[BiCl_3(Te^nBu_2)_3]$ were prepared freshly and a stock solution of each was prepared in anhydrous CH_2Cl_2 (0.033 mmol/mL), henceforward termed 'Se stock' and 'Te stock' respectively. In each of four 10 mm NMR tubes were mixed 1.5 mL of $CDCl_3$ with one of: (i) 1.5 mL of Te stock; (ii) 1.0 mL of Te stock with 0.5 mL of Se stock; (iii) 0.5 mL of Te stock and 1.0 mL of Se stock; (iv) 1.5 mL of Se stock. The colour of the solutions was graduated from red (entirely Te) through orange (mixtures of Se and Te) to yellow (entirely Se) (Figure S7). $^{77}Se\{^1H\}$ and $^{125}Te\{^1H\}$ NMR spectra (as appropriate) were collected at room temperature (Table 3).

A similar approach was adopted for the ternary $Bi_{2-x}Sb_2Te_3$ using samples of $[SbCl_3(Te^nBu_2)_3]$ and $[BiCl_3(Te^nBu_2)_3]$ (Figure S8)

Low Pressure CVD experiments

Physical vapor deposited (PVD) SiO_2 on Si substrates were prepared as described previously.[33] In a typical experiment the reagent, followed by the PVD silica substrate tiles (usually four tiles of 0.5 x 8 x 20 mm) were loaded into a closed-end silica tube in a glovebox. The amount of precursor used was typically between 40-60 mg. The tube was placed horizontally in the furnace such that the precursor was *ca.* 2 cm outside of the heated zone. The tube was evacuated to 0.05 – 0.1 mm Hg. The furnace was then heated to the desired temperature and the temperature was allowed to stabilize. The tube was then repositioned, if necessary, to move the precursor closer to the heated zone to a point where evaporation could be observed. At this point the position of the tube was maintained until the deposition was complete (i.e. the precursor was completely consumed), usually *ca.* 1 h. Once complete, the tube was allowed to cool to room temperature, filled with N_2 and transferred to the glove box where the substrates were removed and stored under N_2 before characterization. For depositions of $Bi_2Se_xTe_{3-x}$ ternary thin films, appropriate ratios of $[BiCl_3(E^nBu_2)_3]$ (E =Se, Te) were first mixed in CH_2Cl_2 and then transferred to the silica CVD tube. The tube was set in the furnace such that the precursor was 2 cm away from the edge of the heated zone. The tube was carefully evacuated (0.05 mm Hg), whereby the CH_2Cl_2 was gradually evaporated, and then the system was ramped up to 550 °C. The tube position was subsequently adjusted so that the precursor was moved towards the hot zone until evaporation was observed. After 1 h, the tube was cooled to room temperature, filled with N_2 and transferred to the glovebox, where the tiles were removed and stored under an N_2 atmosphere prior to analysis. The thin film deposits on the substrates were dark grey in appearance. The highest degree of substrate coverage was found on the tiles closest to the precursor. The films were generally very well adhered to the tiles (except for the Sb_2Se_3 which were very fragile).

Thin Film Characterization

X-ray diffraction (XRD) measurements were carried out using a Rigaku Smartlab diffractometer with a 9 kW Cu-K_α source, parallel line focus incident beam and a DTex250 1D detector. The crystalline phase of the films was determined by matching to a literature XRD pattern and lattice parameters calculated by further optimization of the fit using PDXL.[45] Raman scattering spectra of the deposited films were measured at room temperature on a Renishaw InVia Micro Raman Spectrometer using a helium-neon laser with a wavelength of 633 nm. The incident laser power was adjusted to ~1 mW for all samples. Scanning electron microscopy (SEM) and energy dispersive X-ray (EDX) measurements were performed using a Zeiss EVO LS 25 with an Oxford INCAx-act X-ray detector, or a JEOL JSM 6500 F Field Emission Scanning Electron Microscope with an INCA x-sight 7418 EDX probe with an accelerating voltage of 10 kV. High resolution SEM measurements were carried out with a field emission SEM (Jeol JSM 7500F) at an accelerating voltage of 2 kV.

Van der Pauw and Hall measurements were performed at room temperature on a Nanometrics HL5500PC at 300 K. The latter used a field of 0.5 Tesla. For each measurement, four copper probes with diameter of *ca*. 1 mm were carefully placed on the sample corners. Extra care was taken to ensure linear contact was obtained between each probe and the sample before each measurement.

Results and discussion

Precursor synthesis:

Whilst a number of CVD reagents for Bi_2Se_3 thin film deposition are known (*vide supra*), the previously unknown analogs of the precursor we used to deposit Bi_2Te_3, i.e. $[BiCl_3(Te^nBu_2)_3]$, were prepared with the intention of achieving chemical compatibility between the precursor types. The target compounds, $[BiCl_3(Se^nBu_2)_3]$, $[SbCl_3(Se^nBu_2)_3]$ and $[SbCl_3(Te^nBu_2)_3]$, were prepared using the method illustrated in Scheme 1.

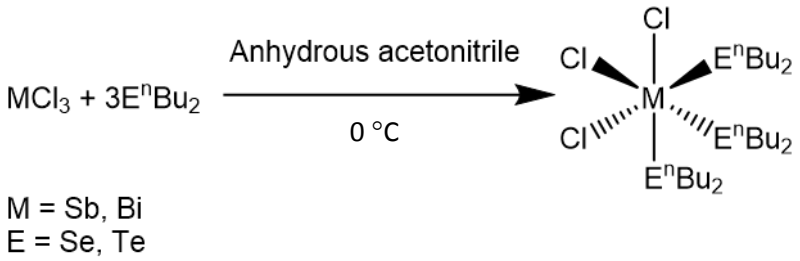

Scheme 1: Synthesis of the precursor complexes

The six-coordinate Sb(III) complexes were isolated in good yields as yellow (Se) and red (Te) oils, respectively, whilst the $[BiCl_3(Se^nBu_2)_3]$ was obtained as an orange oil. Samples were manipulated in an N_2 purged glove box and were stored in a freezer (–18 °C). The selenoether complexes are stable for months at this temperature, whereas the telluroether analog degrades over a few weeks and was therefore prepared freshly prior to CVD experiments. The complexes tend to lose some of the selenoether or telluroether ligands when left for extended periods under high vacuum, leading to products containing a deficit of

chalcogenoether. Consequently, care was taken to prevent this when solvent was being removed during synthesis.

Characterization of new precursors by IR spectroscopy, ^{1}H, ^{13}C{^{1}H}, ^{77}Se{^{1}H} and ^{125}Te{^{1}H} nuclear magnetic resonance (NMR) spectroscopy and microanalysis show the data to be consistent with a distorted octahedral coordination environment. Specifically, infrared (IR) spectroscopy shows strong and broad peaks corresponding to the Bi-Cl and Sb-Cl stretches; at 271 cm^{-1} for [$BiCl_3(Se^nBu_2)_3$], and at 306 and 294 cm^{-1} for [$SbCl_3(Se^nBu_2)_3$].and [$SbCl_3(Te^nBu_2)_3$], respectively, consistent with the literature values of 230 to 280 cm^{-1} for Bi-Cl stretches[46] and 230 to 280 cm^{-1} for Sb-Cl stretches in similar complexes.[47]

The ^{1}H NMR spectra of [$SbCl_3(Se^nBu_2)_3$] and [$SbCl_3(Te^nBu_2)_3$] (CH_2Cl_2) show that the ligand resonances are very little shifted from the 'free' ligand, consistent with the complexes being extensively dissociated in solution. In comparison, the [$BiCl_3(Se^nBu_2)_3$] exhibits a larger high frequency shift, most notably for the CH_2 groups adjacent to the Se donor atom (complex: δ = 3.11; ligand: δ = 2.57 ppm), consistent with BCl_3 being a stronger Lewis acid than $SbCl_3$. The ^{13}C{^{1}H}, ^{77}Se{^{1}H} and ^{125}Te{^{1}H} NMR spectra show similar trends (Table 1).

Table 1: ^{77}Se{^{1}H} and ^{125}Te{^{1}H} NMR spectroscopic data (CH_2Cl_2, 298 K).

Compound	δ(^{77}Se) / ppm	δ(^{125}Te) / ppm
Se^nBu_2	167	–
[$BiCl_3(Se^nBu_2)_3$]	196	–
[$SbCl_3(Se^nBu_2)_3$]	168	–
Te^nBu_2	–	248
[$BiCl_3(Te^nBu_2)_3$]	–	262
[$SbCl_3(Te^nBu_2)_3$]	–	237

LPCVD of binary M_2E_3 (M = Sb, Bi; E = Se, Te) thin films:

LPCVD experiments using each of the four precursors individually, established their suitability for the growth of silvery grey crystalline M_2E_3 films, and these were characterized by grazing incidence XRD, Raman spectroscopy, SEM and EDX analysis (see SI). The refined lattice parameters (Table 2) are in good agreement with literature data for each material. For Bi_2Se_3, LPCVD experiments were typically performed at 550 °C/0.05 mmHg, since at 500 °C a mixture of phases (predominantly BiSe and Bi_3Se_4) was produced, without any evidence for Bi_2Se_3, whereas, increasing the temperature to 600 °C resulted in evaporation of the precursor, but no deposition onto the substrates. The phase pure Bi_2Se_3 films deposited at 550 °C were *ca*. 1 μm thick (Figures S1 and S2).

Table 2. Lattice parameters and electrical data for M_2E_3 films with Bi_2Se_3, Bi_2Te_3 and Sb_2Te_3 adopting the Bi_2Se_3 structure type (*R*-3*mH*) and Sb_2Se_3 the Sb_2S_3 type (*Pnma*).

Precursor	Thin Film Deposit	a / Å	b / Å	c / Å	Type	Resistivity / Ωcm	Mobility μ/ $cm^2V^{-1}S^{-1}$	Carrier Concentration N / cm^{-3}	Ref.
$[BiCl_3(Se^nBu_2)_3]$	Bi_2Se_3	4.092(14)	4.092(14)	28.59(11)	N	8.3×10^{-4}	4.2	2.18×10^{21}	This work
$[BiCl_3(Te^nBu_2)_3]$	Bi_2Te_3	4.378(10) 4.3823(19)	4.378(10) 4.3823(19)	30.46(5) 30.498(17)	N -	$5.65(2) \times 10^{-4}$ -	56.6 -	1.95×10^{20} -	12 This work
$[SbCl_3(Se^nBu_2)_3]$	Sb_2Se_3	11.76(7)	3.938(15)	11.76(6)	-*	$8.4(2) \times 10^4$	-*	-*	This work
$[SbCl_3(Te^nBu_2)_3]$	Sb_2Te_3	4.254(3)	4.254(3)	30.31(5)	P	$1.26(1) \times 10^{-3}$	78.7 ± 1.3	$6.3(1) \times 10^{19}$	This work

* the low density of the orthorhombic Sb_2Se_3 films deposited (see SI) was such that reliable Hall measurements were not possible, hence van der Pauw measurements of resistivity were undertaken.

Energy dispersive X-ray (EDX) spectroscopy analysis shows a Bi: Se ratio of 41.7(0.4):58.3(0.4). Raman analysis (Figure S2b) shows two intense peaks at 130 and 172 cm^{-1}. These can be assigned as the E^2_g (in plane) and the A^2_{1g} (out of plane) vibrational modes, respectively, consistent with values reported in the literature.[48]

The Sb_2Se_3 films were deposited using *ca.* 30 mg of $[SbCl_3(Se^nBu_2)_3]$ at 525, 550 and 575 °C (0.1 mm Hg), leading to complete evaporation of the precursor. The films produced were quite poorly adhered to the substrate (Figure S3), revealing a random orientation of rod- or needle-like crystallites. Quantitative EDX analysis showed that the films were very close to the expected 2:3 Sb:Se stoichiometry (41% Sb : 59% Se); with no evidence for residual Cl. The lower temperature (525 °C) appears best suited for the deposition of Sb_2Se_3 from this precursor. The Raman spectrum (Figure S4b) shows peaks at 125, 150 and 190 cm^{-1}, which represent the E^2_g, A^2_{2u} and A^2_{1g} modes, respectively, from Sb_2Se_3. The E^2_g mode relates to the Se-Se bonds, the A_{1u} to the vibration of Sb-Sb bonds, while the A^2_{1g} mode represents Sb–Se stretching mode of the $SbSe_{3/2}$-pyramids.[13,49,50,51]

Initial depositions using 30-50 mg of freshly prepared $[SbCl_3(Te^nBu_2)_3$ at 450 °C and 500 °C onto SiO_2, with the precursor positioned about 2 cm from the hot zone and gradually moved closer until sublimation was observed. In all cases this resulted in the co-deposition of Sb_2Te_3 and crystalline tellurium. Under these conditions, it appears that some of the telluroether ligand may be distilled from the precursor across the hot zone, producing crystalline tellurium. Adaptation of the method, where the CVD tube was repositioned such that once the required furnace temperature was reached, the precursor was moved rapidly to the edge of the hot zone, allowed for 'flash evaporation' of the precursor. This allowed Sb_2Te_3 films to be obtained without co-depositing elemental tellurium. At 450 °C the small crystallites deposited are very scattered and the film is not continuous (Figure S5a). Increasing the temperature to 500 °C to increase nucleation led to

continuous films of Sb_2Te_3 being produced. SEM analysis of the films produced at 450 °C shows the crystallites to be *ca.* 100 nm in diameter, whilst those grown at 500 °C are *ca.* 1 µm across, and the substrate coverage is much higher (Figure S5b). In comparison with Sb_2Te_3 films deposited from $MeSb(Te^nBu_2)_2$,[13] the films deposited from the new $[SbCl_3(Te^nBu_2)_3]$ precursor do not show any significant preferred orientation, with some crystallites lying flat and some perpendicular to the substrate. The elemental composition of the Sb_2Te_3 film was also probed by EDX analysis, showing an Sb:Te ratio of 38%:62%, i.e. within experimental error of that expected for Sb_2Te_3. There is no evidence for Cl incorporation into the film. The Raman spectrum (Figure S6b) of the film shows peaks at 120, 140 and 165 cm^{-1}, attributed to the E_{2g}, A_{2u} and A_{1g} vibrational modes expected from Sb_2Te_3.[52]

We have shown previously that Bi_2Te_3 can be selectively deposited into the TiN wells of lithographically patterned TiN/SiO_2 substrates using the precursor $[BiCl_3(Te^nBu_2)_3]$.[12] Selective deposition of Sb_2Te_3 was therefore attempted using ~5 mg of $[SbCl_3(Te^nBu_2)_3]$ at 723 K. SEM images revealed that Sb_2Te_3 can indeed be deposited preferentially into the TiN wells of a lithographically patterned TiN/SiO_2 substrate (Figure 1a), with very few crystallites deposited outside of the TiN wells. Quantitative EDX analysis revealed both Sb and Te to be present with a Sb : Te ratio of 41:59. Grazing incidence XRD data are also consistent with R-3mh Sb_2Te_3 (Figure 1b)

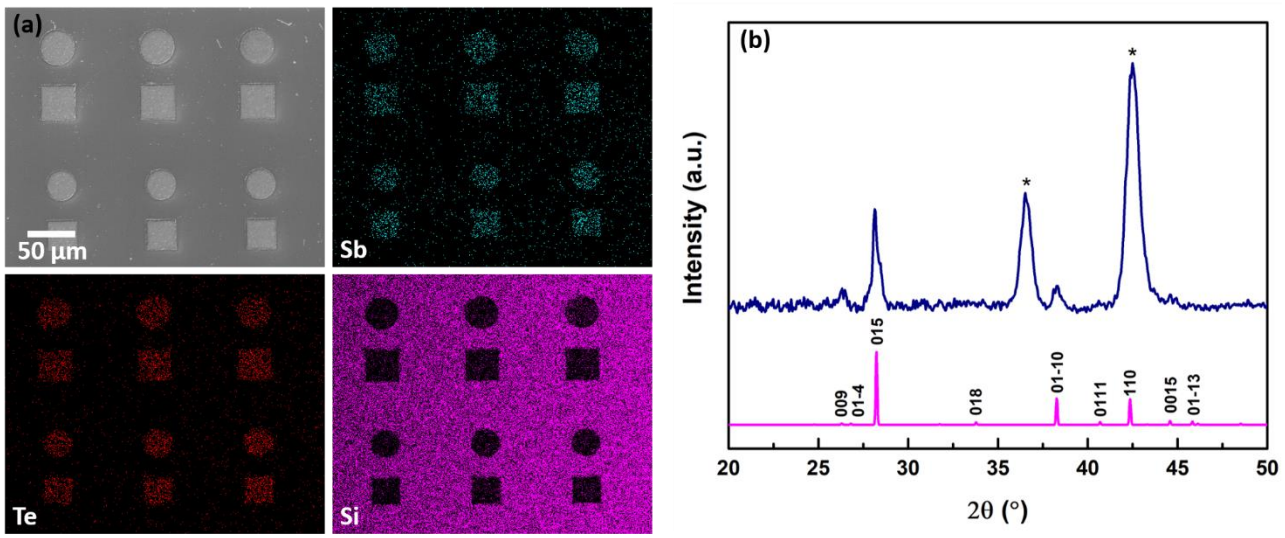

Figure 1: (a) SEM image and (b) grazing incidence XRD pattern from Sb_2Te_3 selectively deposited from $[SbCl_3(^nBu_2Te)_3]$ into 10 µm TiN holes and an indexed bulk pattern of Sb_2Te_3.[53] The TiN substrate peaks are indicated by *.

Electrical measurements on binary M_2E_3 films:

The electrical properties of the binary M_2E_3 films were investigated by Hall measurements performed at room temperature. Results show that Sb_2Te_3 is a p-type semiconductor, whilst and Sb_2Se_3, Bi_2Se_3 and Bi_2Te_3 are n-type semiconductors. Electrical measurements are shown below in Table 2.

Sb_2Te_3 was observed to have a very low resistivity (1.26 x 10^{-3} Ω cm), comparable to that of Sb_2Te_3 films deposited by other methods, including LPCVD from $[MeSb(Te^nBu_2)_2]$ (9.9 x 10^{-4} Ω cm),[13] by molecular beam

epitaxy (5.9 x 10^{-4} Ω cm)[11] and by atomic layer deposition (9.6 x 10^{-3} Ω cm).[14] Hall electrical measurements show that Bi_2Se_3 is a n-type semiconductor with a low resistivity of 8.3 x 10^{-4} Ωcm. The mobility is 4.2 cm^2/C and the carrier density is 2.18 x 10^{21} cm^{-3}.

***LPCVD of ternary $Bi_2(Se_{1-x}Te_x)_3$ thin films*:**

Our approach to deposit thin films of the ternary chalcogenide, $Bi_2(Se_{1-x}Te_x)_3$, exploits the inherent high lability of Bi(III) complexes with neutral donor ligands in solution. We have utilized the rapid ligand substitution kinetics of $[BiCl_3(E^nBu_2)]$ (E = Se, Te) to create mixed telluroether/selenoether complexes of $BiCl_3$ by combining various ratios of the precursors in CH_2Cl_2 solution prior to the CVD experiments. The relatively similar temperatures required for LPCVD of each of the binary M_2E_3 phases from this homologous pair of precursors was also promising for the LPCVD of the required $Bi_2(Se_{1-x}Te_x)_3$ ternary phase. At first sight, the need for a higher temperature for the Bi_2Se_3 deposition (550 °C) from $[BiCl_3(Se^nBu_2)_3]$ in comparison to that for LPCVD growth of Bi_2Te_3 (450 °C) was unexpected. However, this most likely reflects the presence of the weaker Te–C bonds in the latter (*cf.* the Se–C bonds in $[BiCl_3(Se^nBu_2)_3]$), arising from the orbital energy mismatch of the C and Te atoms. Hence, while the volatility of the higher MWt $[BiCl_3(Te^nBu_2)_3]$ precursor is expected to be lower than for the $[BiCl_3(Se^nBu_2)_3]$ precursor, this is apparently offset by its lower thermal stability.

To test the concept that these two precursors would be compatible for the optimization of the target ternary $Bi_2Te_{3-x}Se_x$ phase by LPCVD, we initially studied the solution behaviour of $[BiCl_3(Te^nBu_2)_3]$ and $[BiCl_3(Se^nBu_2)_3]$, and mixtures thereof, by $^{77}Se\{^1H\}$ and $^{125}Te\{^1H\}$ NMR spectroscopy in CH_2Cl_2 solution. The results are presented in Figure S7. Each of solutions (**i**) to (**iv**) gave only one resonance at room temperature. Introducing increasing amounts of $[BiCl_3(Te^nBu_2)_3]$ into a solution of $[BiCl_3(Se^nBu_2)_3]$ leads to $\delta(^{77}Se)$ progressively shifting to lower frequency, while $\delta(^{125}Te)$ moves to higher frequency (*cf.* that of the individual parent complexes). Lowering the temperature to –80 °C leads only to slight broadening of the resonances for each of the parent complexes (i) and (iv), and this was replicated for the mixed Se/Te samples ((**ii**) and (**iii**)). This behaviour is consistent with rapid ligand scrambling in CH_2Cl_2 solution and the high lability of the bismuth trichloride acceptor, suggesting that the species present in solution are of the form $[BiCl_3(Te^nBu_2)_{3-x}(Se^nBu_2)_x]$.

A series of LP CVD experiments was then undertaken by mixing different ratios of the two precursors in CH_2Cl_2 to produce $[BiCl_3(Te^nBu_2)_{3-x}(Se^nBu_2)_x]$ with different values of x (from 0 to 3). Depositions were performed at 550 °C/0.05 mmHg onto SiO_2-coated silicon substrates. In each case, reflective silvery films were obtained.

The EDX analyses (Figure 2) revealed that the %Te content increases with increasing Te precursor content, with a concomitant decrease in the %Se present, as expected. These data indicate good control of the composition of the $Bi_2(Se_{1-x}Te_x)_3$ ternary material using the $[BiCl_3(Te^nBu_2)_3]/[BiCl_3(Se^nBu_2)_3]$ precursor system. It is worth noting that the %Te does not increase linearly with the Te precursor content. In particular, it demonstrates an enhancement in Te deposition. The dotted lines in Figure 3b represent the

theoretical %content value calculated from the Te precursor content with an enhancement factor α of 2.5. This enhanced deposition of Te could be accounted for by the lower thermal stability of the $[BiCl_3(Te^nBu_2)_3]$ precursor due to the weaker Te–C bonds (as discussed above).

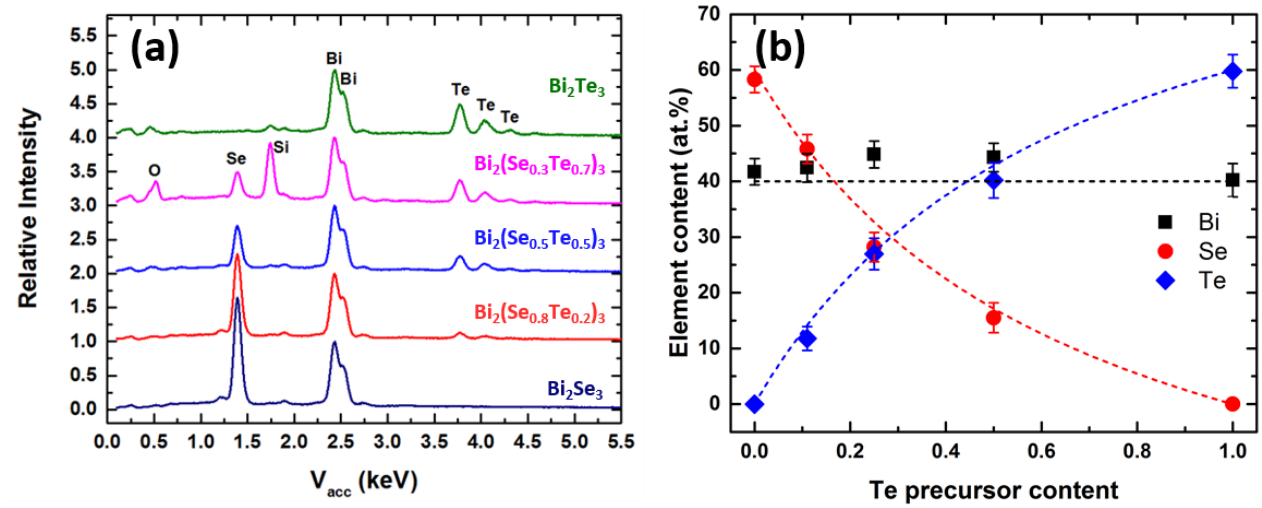

Figure 2 (a) EDX spectra and (b) relationship between film composition and fraction of $[BiCl_3(Te^nBu_2)_3]$ used in the deposition of ternary $Bi_2(Se_{1-x}Te_x)_3$ films.

SEM (Figure 3) analysis shows that the ternary films, like the binary parent materials, are polycrystalline, with good coverage across the substrate. In each case film thicknesses of *ca.* 1 μm were obtained. The hexagonal crystallites are clearly visible, although their orientation varies; for the Bi_2Se_3 films, the crystallites appear to be aligned perpendicular to the substrate, whereas in the ternary and Bi_2Te_3 films most of the crystallites tend to lie parallel to the surface.

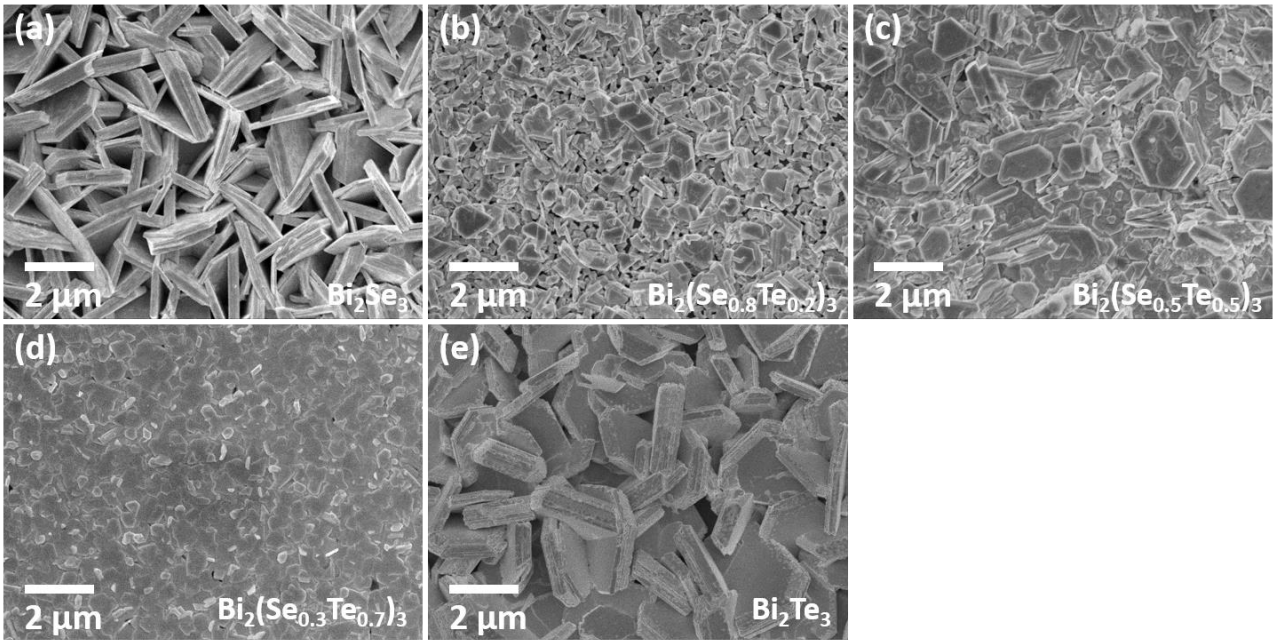

Figure 3 SEM images showing the morphologies of the Bi_2Se_3 (a), Bi_2Te_3 (e) and (c-d) ternary $Bi_2(Se_{1-x}Te_x)_3$ films deposited by LPCVD under similar conditions (550 °C/0.05 mmHg) onto SiO_2-coated silicon substrates.

The phase purity and crystal structure of the as-deposited films have been identified by grazing incidence XRD analysis and the patterns are shown in Figure 4a. All five films are isostructural with no detectable impurities from any other phase. A systematic shift of all the characteristic peaks has been observed with increasing Te composition. Figure 4b presents the enlarged view of the trend observed for the 015 diffraction peak. Noticeable broadening of this peak for the $Bi_2(Se_{0.8}Te_{0.2})_3$, $Bi_2(Se_{0.5}Te_{0.5})_3$, $Bi_2(Se_{0.3}Te_{0.7})_3$ films can be observed, which implies that disorder has been introduced into the crystal structures due to Te doping. This disorder can also be characterized by the decrease of the crystallite sizes for these three ternary compositions observed in Figure 3. The lattice parameters (*a* and *c*) of all five compositions are refined against the Bi_2Se_3 phase from the ICSD.[54] Linear increases of both *a* and *c* with increasing Te content are observed (Figure 4c), consistent with Vegard's law, i.e. well distributed solid solutions of the ternary $Bi_2(Se_{1-x}Te_x)_3$, and produce a linear lattice parameter trend.

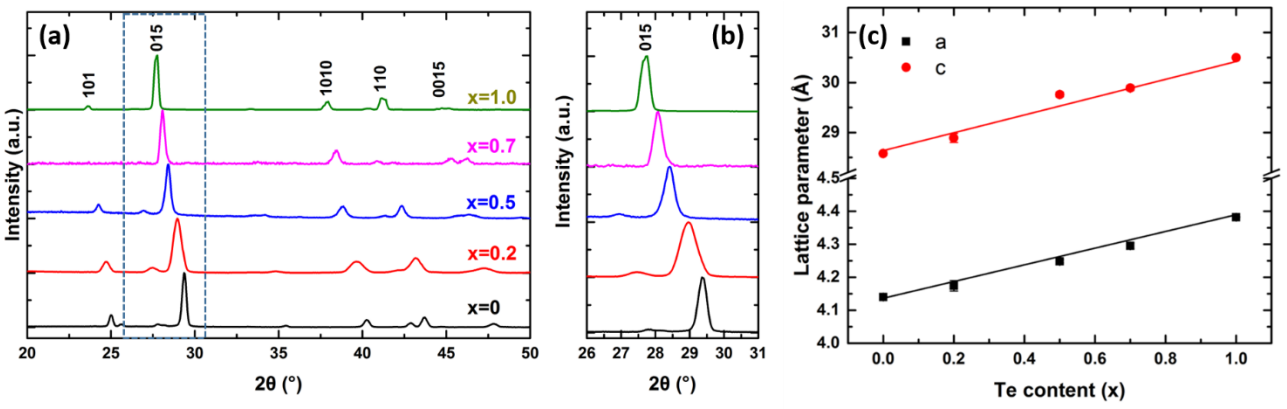

Figure 4. (a) XRD patterns of as-deposited $Bi_2(Se_{1-x}Te_x)_3$ films with x ranging from 0 to 1; (b) expanded XRD patterns showing the systematic shift of the 015 peak; (c) refined lattice parameters (see Table S1) as a function of the Te content for different as-deposited $Bi_2(Se_{1-x}Te_x)_3$ films.

The vibrational properties of the as-deposited $Bi_2(Se_{1-x}Te_x)_3$ films were also studied by Raman spectroscopy. The spectra are shown in Figure 5, where peaks are fitted using the Gaussian equation. For Bi_2Te_3 (Figure 5a), two peaks positioned at 129 and 171 cm^{-1} can be assigned as E_g^2 (in-plane) and A_{1g}^2 (out-of-plane) modes, respectively, similar to previous reported values.[47] These two vibrational modes have also been detected in the other four films, although shifts towards low wavenumbers were observed with increasing Te content (Figure 5f). This can be explained by the substitution of Te into Se sites, which modifies the lattice vibrations and the electron-phonon interactions within $Bi_2(Se_{1-x}Te_x)_3$ structure. As Te atoms are heavier than the Se atoms, they vibrates less when interacting with the laser, producing Raman bands with higher wavenumber. Similar shifts have been reported.[39,40] An additional peak at *ca.* 120 cm^{-1} is detected for $Bi_2(Se_{0.3}Te_{0.7})_3$ and Bi_2Te_3 (Figure 5d and e), ascribed to the A_{1u} mode, which is IR-active. The appearance of this peak implies the breaking of the crystal symmetry in the third dimension due to the limited thickness and the presence of the interfaces.[55,56]

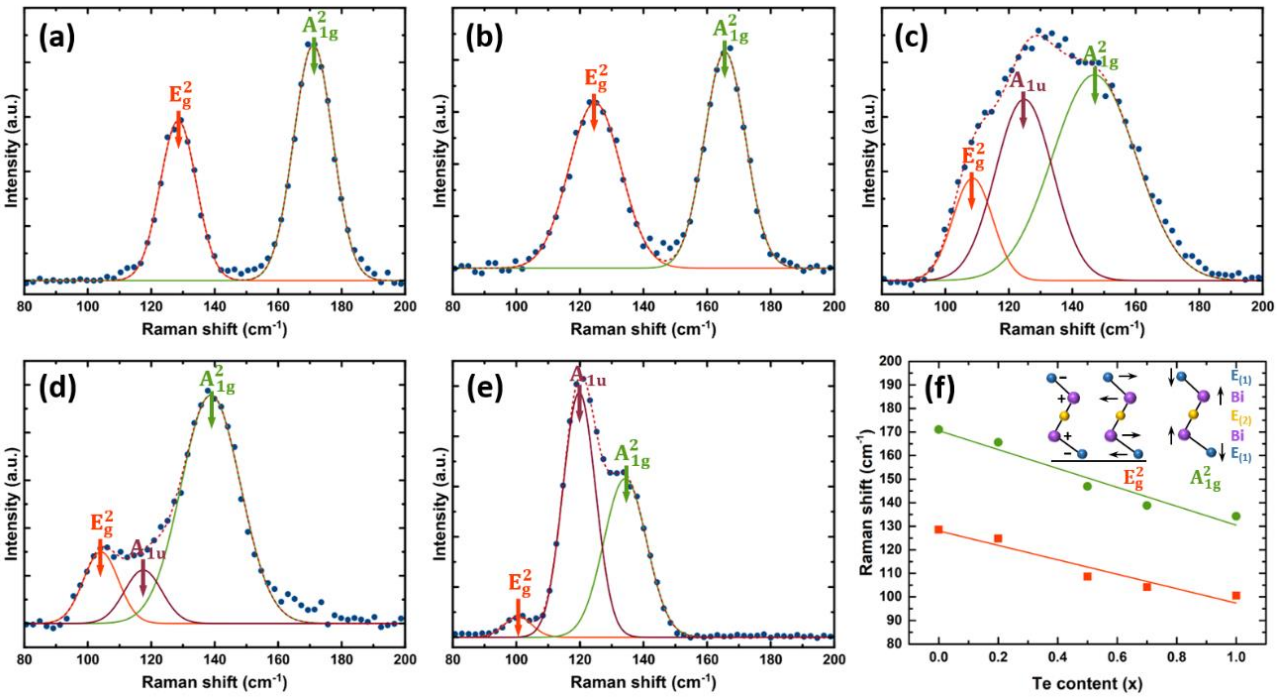

Figure 5. (a)-(e) Raman spectra of as-deposited $Bi_2(Se_{1-x}Te_x)_3$ films with x ranging from 0 to 1. (f) phonon frequencies as a function of Te composition. The inset provides the schematic diagrams for the two Raman-active modes.

The electrical behaviour of the series is shown in Figure 6. All films are measured to be n-type semiconductors with resistivities in the range of mΩ·cm. The resistivity demonstrates a noticeable maximum for Te content x = 0.7, similar to the trend reported previously.[57]

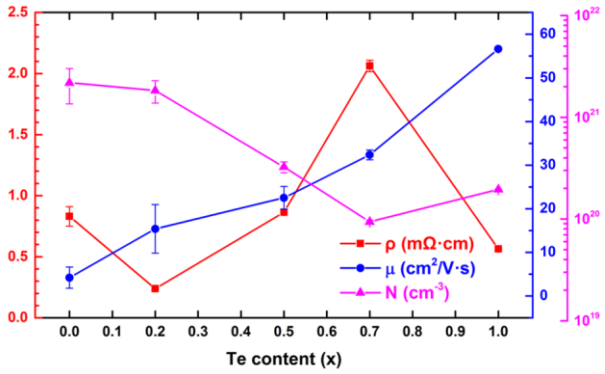

Figure 6. Resistivity of as-deposited $Bi_2(Se_{1-x}Te_x)_3$ films with x ranging from 0 to 1.

LPCVD of $(Bi_{1-x}Sb_x)_2Te_3$ thin films

To ascertain the compatibility of the two precursors required for the target ternary $(Bi_{1-x}Sb_x)_2Te_3$ thin films, different ratios of $[MCl_3(Te^nBu_2)_3]$ (M = Bi and Sb) were analysed by $^{125}Te\{^1H\}$ NMR spectroscopy in CH_2Cl_2. In all cases, just one Te resonance is observed, consistent with the Te^nBu_2 ligands being labile and freely exchanging between the two weakly Lewis acidic metal centres. A gradual change in chemical shift is observed with increasing Bi content, from 237 ppm for pure $[SbCl_3(Te^nBu_2)_3]$, to 262 ppm for pure $[BiCl_3(Te^nBu_2)_3]$.

In order to deposit the target ternary $(Bi_{1-x}Sb_x)_2Te_3$ films, various ratios the $[BiCl_3(Te^nBu_2)_3]$ and $[SbCl_3(Te^nBu_2)_3]$ precursors were combined. In a typical LPCVD experiment, *ca.* 60 mg total mass of the reagents were combined in the chosen ratio, and the deposition was performed at 500 °C onto SiO_2 substrates, leading to silver-grey films across 4-6 substrates. Temperature profiling of the furnace revealed that when set to 500 °C, there was a temperature gradient from 270 °C at the edge of the furnace to 496 °C in the centre. Analysis of the films by XRD, EDX, SEM and Raman spectroscopy revealed that there was a variation in composition across the substrates, with increasing antimony content at higher deposition temperatures. The following analysis focuses on the films with the best coverage and showing a clear compositional variation with deposition temperature (across a 8 °C range from 474 – 482 °C), with the composition switching from Bi-rich at the cooler end, to Sb rich at the hotter end.

EDX analysis (Figure 7) was used to map the composition along the length of the sample (as a function of deposition temperature). Figure 7b**Error! Reference source not found.** shows the change in %Sb content with temperature across the substrate; moving from lower to higher temperature the Bi content decreases. It also shows that the Sb-rich phases are deposited within a very narrow temperature range. It is clear that Bi_2Te_3 is more easily deposited at lower temperatures than Sb_2Te_3 and consequently, the bismuth content in the vapour phase of the precursor is depleted in the early stages of the hot zone which means it does not reach the substrates at higher temperatures.

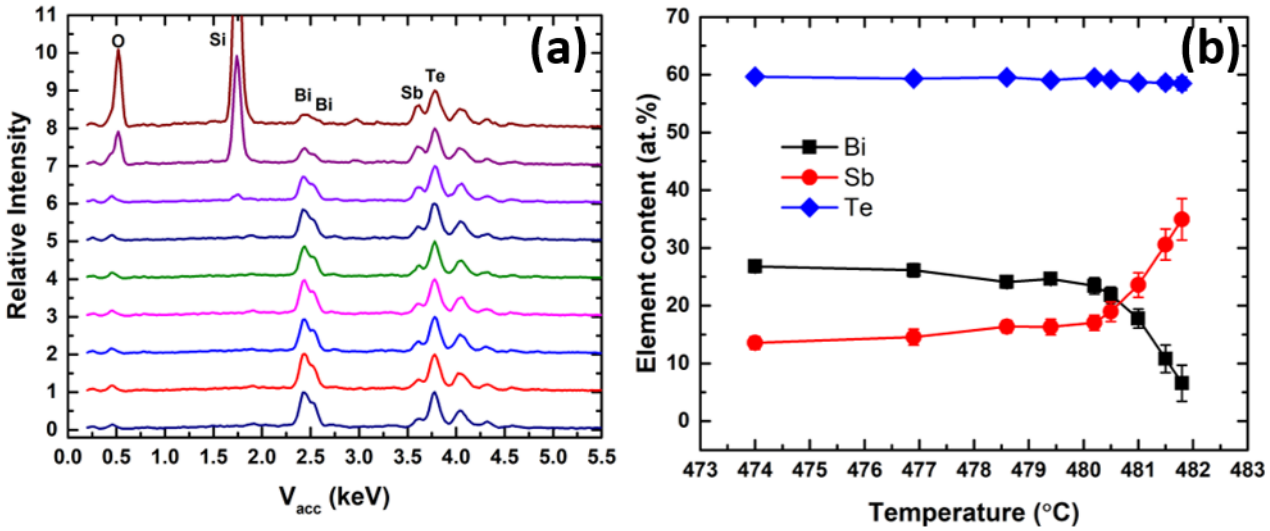

Figure 7: (a) EDX spectra and (b) relationship between $(Bi_{1-x}Sb_x)_2Te_3$ film composition and the increasing temperature of deposition.

SEM images (Figure 8) taken at three positions across the substrate show that the morphology is rather different from the regular hexagonal morphology observed for either Bi_2Te_3 or Sb_2Te_3. Moving along the substrate to the more antimony rich phase, individual irregularly-shaped plate-like crystallites are observed, rather than regular hexagons.

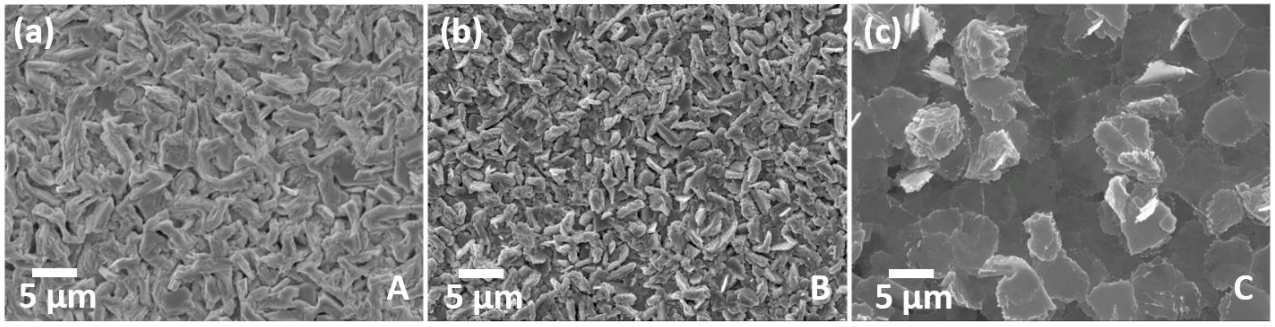

Figure 8: SEM images of three regions (A-C) of the film deposited from a 1:1 ratio of $[SbCl_3(Te^nBu_2)_3]$ and $[BiCl_3(Te^nBu_2)_3]$ from Sb poor (a) to Sb rich (c).

Grazing incidence XRD data (Figure 9) are consistent with a single phase (with no elemental Te) and show the reflections gradually shift from a lower 2θ value for Bi_2Te_3 to a higher 2θ value with increasing antimony content, as expected. The variation in the lattice parameters with antimony content is shown in Figure 9c. Whilst the lattice parameter change is smaller in this system, there is an approximately linear trend, consistent with Vegard behavior.

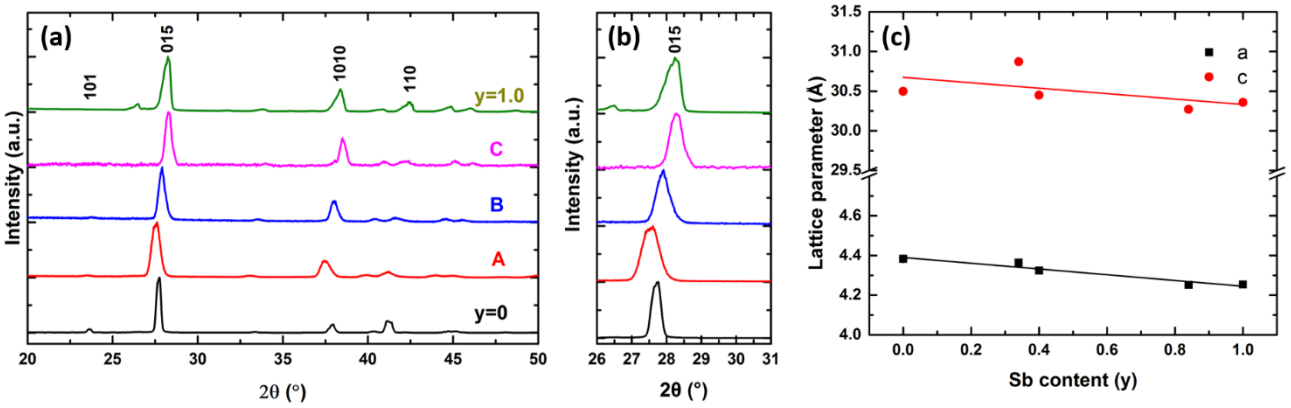

Figure 9: (a) Grazing incidence XRD patterns from 3 positions (Sb poor to Sb rich) of a ternary sample deposited from a 1:1 ratio of $[SbCl_3(Te^nBu_2)_3]$ and $[BiCl_3(Te^nBu_2)_3]$, together with the binary phases (Sb_2Te_3 and Bi_2Te_3). Position A: a = 4.370(11) and c = 30.80(8) Å, Position B: a = 4.327(8) and c = 30.54(8) Å, Position C: a = 4.249(9) and c = 30.29(8) Å. (b) expanded XRD patterns showing the systematic shift of the 015 peak; (c) refined lattice parameters as a function of the Sb content for different as-deposited $(Bi_{1-y}Sb_y)_2Te_3$ films.

The composition of the film was also mapped with Raman spectroscopy, as depicted in Figure . This shows the shift in peaks from Bi_2Te_3 to Sb_2Te_3. The E_g^2 vibrational mode shifts from 100 to 120 cm^{-1} and the A_{1g}^2 mode shifts from 134 to 167 cm^{-1} showing the change in composition of the solid solution of the ternary phase. This is consistent with Raman spectra of $(Bi_{1-x}Sb_x)_2Te_3$ deposited by solvothermal synthesis[58] and MBE.[38]

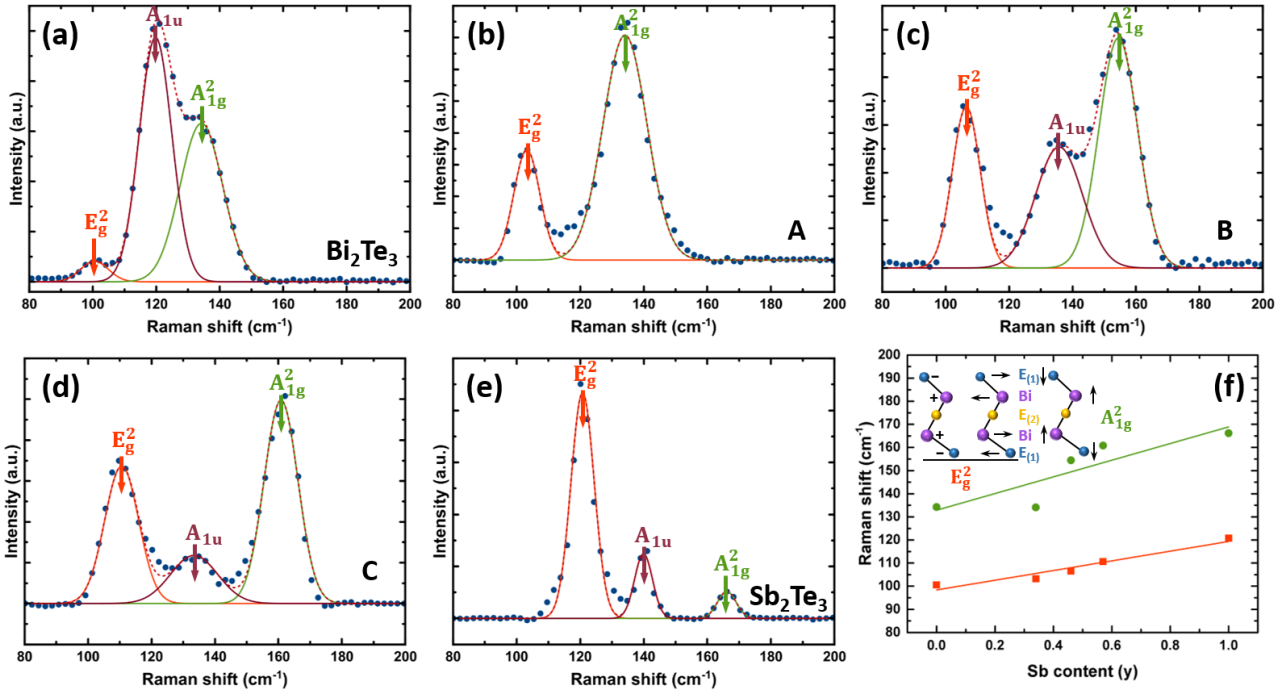

Figure 10: Raman spectra from 3 positions (Sb poor to Sb rich) of a ternary $(Bi_{1-y}Sb_y)_2Te_3$ sample deposited from a 1:1 ratio of $[SbCl_3(Te^nBu_2)_3]$ and $[BiCl_3(Te^nBu_2)_3]$, together with the binary phases (Sb_2Te_3 and Bi_2Te_3).

Conclusions

This work presents a chemically compatible series of molecular precursors suitable for the growth of binary M_2E_3 (M = Sb, Bi; E = Se, Te) thin films on silica by LPCVD. Moreover, their suitability to be combined in differing ratios to allow the LPCVD of ternary $Bi_2(Se_{1-x}Te_x)_3$ and $(Bi_{1-y}Sb_y)_2Te_3$ films with good compositional control, as well-distributed solid solutions (following Vegard behaviour), is established. In the case of $Bi_2(Se_{1-x}Te_x)_3$, the ternary composition is largely governed by the relative ratios of the precursors used, whilst for $(Bi_{1-y}Sb_y)_2Te_3$, the composition is influenced by the deposition temperature. Compositional control across the ternary phase is significant for tuning the functional properties of the V-VI materials for use in thermoelectric devices or topological insulators. This, coupled with the ability of this precursor system to allow M_2E_3 film deposition selectively onto particular regions of lithographically patterned substrates, suggests that using this set of precursors in a CVD based approach offers considerable promise for the fabrication of thin film micro-thermoelectric generators. This will be the basis of our future work.

Acknowledgements

We thank the Science and Technology Research Council, UK (STFC) for funding this work through ST/L003376/1 and ST/P00007X/1 and the Engineering and Physical Sciences Research Council (EPSRC) for a Case Award (to S.L.H.) through EP/M50662X/1. We also gratefully acknowledge funding for thin film diffraction and NMR instrumentation from the EPSRC through EP/K00509X, EP/K009877/1 and EP/K039466/1. C.G. thanks the Royal Society (London) for a Newton International Alumnus Award.

Supporting Information

The Supporting Information contains SEM, XRD and Raman data for each of the binary materials produced in this work and $^{77}Se\{^1H\}$ and $^{125}Te\{^1H\}$ NMR spectroscopic data associated with the precursor combinations.

Conflicts of Interest

The authors declare no competing financial interest.

References

[1] Madelung, O., *Semiconductors: Data Handbook vol 14*, Springer Berlin Heidelberg, Berlin Heidelberg, **2004**.
[2] Harman, T. C.; Paris, B.; Miller, S. E.; Goering, H. L., *J. Phys. Chem. Solids*, **1957**, *2*, 181–190.
[3] Snyder, G. J.; Toberer, E. S., *Nat. Mater.*, 2008, **7**, 105-114.
[4] Bell, L. E., *Science*, **2008**, *321*, 1457–1461.
[5] Kutasov, V. A.; Lukyanova, L. N.; Vedernikov, M. V. in Thermoelectrics Handbook: Macro to Nano, ed. Michael, R. D., CRC Press, **2006**, ch. 37.
[6] Vineis, C. J.; Shakouri, A.; Majumdar, A.; Kanatzidis, M.. G., *Adv. Mater*., **2010**, *22*, 3970–3980.
[7] Al Bayaz, A.; Giani, A.; Foucaran, A.; Pascal-Delannoy, F.; Boyer, A., *Thin Solid Films*, **2003**, *441*, 1–5.
[8] You, H.; Hyub Baek, S.; Kim, K.-C.; Kwon, O.-J.; Kim, J.-S.; Park, C., *J. Cryst. Growth*, **2012**, *346*, 17–21. check
[9] Wang, X.; He, H.; Wang, N.; Miao, L., *Appl. Surf. Sci.*, **2013**, *276*, 539–542.
[10] Rashid, M. M.; Cho, K. H.; Chung, G.-S., *Appl. Surf. Sci.*, **2013**, *279*, 23–30.

[11] Peranio, N.; Winkler, M.; Aabdin, Z.; König, J.; Böttner, H.; Eibl, O., *Phys. Status Solidi*, **2012**, *209*, 289–293.
[12] Benjamin, S. L.; de Groot, C. H.; Gurnani, C.; Hector, A. L.; Huang, R.; Koukharenko, E.; Levason, W.; Reid, G., *J. Mater. Chem. A*, **2014**, *2*, 4865–4869.
[13] Benjamin, S. L.; de Groot, C. H.; Hector, A. L.; Huang, R.; Koukharenko, E.; Levason, W.; Reid, G., *J. Mater. Chem. C*, **2015**, *3*, 423–430.
[14] Zastrow, S.; Gooth, J.; Boehnert, T.; Heiderich, S.; Toellner, W.; Heimann, S.; Schulz, S.; Nielsch, K., *Semicond. Sci. Technol.*, **2013**, *28*, 35010 (6 pages].
[15] Fan, P.; Zheng, Z. H.; Liang, G. X.; Zhang, D. P.; Cai, X. M., *J. Alloys Compd.*, **2010**, *505*, 278–280.
[16] Gilbert, L.; Van Pelt, B.; Wood, C., *J. Phys. Chem. Solids*, **1974**, *35*, 1629–1632.
[17] Zhou, Y.; Leng, M.; Xia, Z.; Zhong, J.; Song, H.; Liu, X.; Yang, B.; Zhang, J.; Chen, J.; Zhou, K.; Han, J.; Cheng, Y.; Tang, J., *Adv. Energy Mater.*, **2014**, *4*, 1301846-53.
[18] Chen, C.; Bobela, D. C.; Yang, Y.; Lu, S.; Zeng, K.; Ge, C.; Yang, B.; Gao, L.; Zhao, Y.; Beard, M. C., Tang, J., *Front. Optoelectron.*, **2017**, *10*, 18–30.
[19] Choi, Y. C.; Mandal, T. N.; Yang, W. S.; Lee, Y. H.; Im, S. H.; Noh, J. H.; Il Seok, S., *Angew. Chem. Int. Ed.*, **2014**, *53*, 1329–1333.
[20] Liu, X.; Chen, J.; Luo, M.; Leng, M.; Xia, Z.; Zhou, Y.; Qin, S.; Xue, D. J.; Lv, L.; Huang, H.; Niu, D.; Tang, J., *ACS Appl. Mater. Interfaces*, **2014**, *6*, 10687–10695.
[21] Zhang, H.; Liu, C.-X.; Qi, X.-L.; Dai, X.; Fang, Z.; Zhang, S.-C., *Nat. Phys.*, **2009**, *5*, 438–442.
[22] Guo, Y.; Liu, Z.; Peng, H., *Small*, **2015**, *11*, 3290–3305.
[23] Zastrow, S.; Gooth, J.; Boehnert, T.; Heiderich, S.; Toellner, W.; Heimann, S.; Schulz, S.; Nielsch, K., *Semicond. Sci. Technol.*, **2013**, *28*, 35010 (6 pages).
[24] Jones, A. C.; Hitchman, M. L., in *Chemical Vapour Deposition: Precursors*, (Eds: Jones, A. C.; Hitchman, M. L.), The Royal Society of Chemistry, **2009**, 1-36.
[25] Giani, A.; Boulouz, A.; Delannoy, F. P.; Foucaran, A.; Boyer, A.; Aboulfarah, B.; Mzerd, A., *J. Mater. Sci. Lett.*, **1999**, *18*, 541–543.
[26] Kim, J. H.; Jung, Y. C.; Suh, S. H.; Kim, J. S., *J. Nanosci. Nanotechnol.*, **2006**, *6*, 3325–3328.
[27] Waters, J.; Crouch, D.; Raftery, J.; O'Brien, P., *Chem. Mater.*, **2004**, *16*, 3289–3298.
[28] Waters, J.; Crouch, D.; O. Brien, P.; Park, J., **2003**, *4*, 599–602.
[29] Garje, S. S.; Eisler, D. J.; Ritch, J. S.; Afzaal, M.; O'Brien, P.; Chivers, T., *J. Am. Chem. Soc.*, **2006**, *128*, 3120–3121.
[30] Sharma, R. K.; Kedarnath, G.; Jain, V. K.; Wadawale, A.; Nalliath, M.; Pillai, C. G. S.; Vishwanadh, B., *Dalton Trans.*, **2010**, *39*, 8779–8787.
[31] Huang, R.; Benjamin, S. L.; Gurnani, C.; Wang, Y.; Hector, A. L.; Levason, W.; Reid, G.; de Groot, C. H., *Sci. Rep.*, **2016**, *6*, 27593 (10 pages).
[32] Reid, S. D.; Hector, A. L.; Levason, W.; Reid, G.; Waller, B. J.; Webster, M., *Dalton Trans*., **2007**, 4769-4777.
[33] de Groot, C. H.; Gurnani, C.; Hector, A. L.; Huang, R.; Jura, M.; Levason, W.; Reid, G.. *Chem. Mater.,* **2012**, *24*, 4442–4449.
[34] George, K.; de Groot, C. H.; Gurnani, C.; Hector, A. L.; Huang, R.; Jura, M.; Levason, W.; Reid, G., *Chem. Mater.*, **2013**, *25*, 1829-1836.
[35] Benjamin, S. L.; de Groot, C. H.; Gurnani, C.; Hector, A. L.; Huang, R.; Ignatyev, K.; Levason, W.; Pearce, S. J.; Thomas, F.; Reid, G., *Chem. Mater.*, **2013**, *25*, 4719-4724.
[36] R. Venkatasubramanian, E. Siivola, T. Colpitts and B. O'Quinn, *Nature*, **2001**, *413*, 597–602.
[37] Guo, X.; Jia, X.; Jie, K.; Sun, H.; Zhang, Y.; Sun, B.; Ma, H., *CrystEngComm*, **2013**, *15*, 7236–7242.
[38] Weyrich, C.; Drögeler, M .; Kampmeier, J.; Eschbach, M.; Mussler, G.; Merzenich, T.; Stoica, T.; Batov, I. E.; Schubert, J.; Plucinski, L., *J. Phys. Cond. Matter*, **2016**, *28*, 495501.

[39] Hong, M.; Chasapis, T. C.; Chen, Z.-G.; Yang, L.; Kanatzidis, M. G.; Snyder, J.; Zou, J., *ACS Nano,* **2016**, *10*, 4719–4727.

[40] Soni, A.; Yanyuan, Z.; Ligen, Y.; Aik, M. K. K.; Dresselhaus, M. S.; Ziong, Q., *Nano Lett.,* **2012**, *12*, 1203–1209.

[41] Mi, J.-L.; Norby, P.; Bremholm, M.; Iversen, B. B., *Chem. Mater.*, **2017**, *29*, 5070–5079.

[42] Xu, B.; Feng, T.; Agne, A. T. ; Zhou, L. ; Ruan, Z.; Snyder, G. J.; Wu, Y., *Angew. Chem. Int. Ed.*, **2017**, *56*, 3546–3551.

[43] Gulliver, D. J.; Hope, E. G.; Levason, W.; Murray, S. G.; Potter, D. M.; Marshall, G. L., *J. Chem. Soc., Perkin Trans. 2,* **1984**, 429–434.

[44] Hope, E. G.; Kemmitt, T.; Levason, W., *Organometallics*, **1988**, *7*, 78–83.

[45] Grazulis, S.; Chateigner, D.; Downs, R. T.; Yokochi, A. F.; Quiros, M.; Lutterotti, L.; Manakova, E.; Butkus, J.; Moeck, P.; Le Bail, A., *J. Appl. Crystallogr*., **2009**, *42*, 726–729.

[46] (a) Barton, A. J.; Genge, A. R. J.; Levason, W.; Reid, G., J. Chem. Soc., Dalton Trans., 2000, 859–865; (b) Levason, W.; Hill. N. J.; Reid, G., *J. Chem. Soc., Dalton Trans*., **2002**, 4316–4317.

[47] (a) Barton, A. J.; Hill, N. J.; Levason, W.; Patel, B.; Reid, G., *Chem. Commun*., **2001**, 95–96; (b) Barton, A. J.; Hill, N. J.; Levason, W.; Reid, G., *J. Chem. Soc., Dalton Trans.*, **2001**, 1621–1627.

[48] Zhang, J.; Peng, Z.; Soni, A.; Zhao, Y.; Xiong, Y.; Peng, B.; Wang, J.; Dresselhaus, M. S.; Xiong, Q., *Nano Lett.*, **2011**, *11*, 2407–2414.

[49] Wang, J.; Deng, Z.; Li, Y., *Mater. Res. Bull.*, **2002**, *37*, 495–502.

[50] Bera, A.; Pal, K.; Muthu, D. V. S.; Sen, S.; Guptasarma, P.; Waghmare, U. V.; Sood, A. K., *Phys. Rev. Lett.*, **2013**, *110*, 1–5.

[51] Ivanova, Z. G.; Cernoskova, E.; Vassilev, V. S.; Boycheva, S. V., *Mater. Lett.*, **2003**, *57*, 1025–1028.

[52] Sosso, G. C.; Caravati, S.; Bernasconi, M., *J. Phys. Condens. Matter*, **2009**, *21*, 95410 (6 pages).

[53] Anderson, B. Y. T. L.; Krause, H. B., *Acta Cryst.*, **1974**, *B30*, 1307–1310.

[54] ICSD: Inorganic Crystal Structure Database (ICSD), Fachinformationszentrum Karlsruhe (FIZ), accessed via the EPSRC funded National Chemical Database Service hosted by the Royal Society of Chemistry.

[55] D. Teweldebrhan, V. Goyal and A. A. Balandin, *Nano Lett.*, **2010**, *10*, 1209-1218.

[56] Shahil, K. M. F.; Hossain, M. Z.; Teweldebrhan, D.; Balandin, A. A., *Appl. Phys. Lett.,* **2010**, *96***,** 2–4.

[57] Akrap, A.; Ubaldini, A.; Giannini, E.; Forro, L., *EPL*, **2014**, *107*, 57008.

[58] Zhang, C.; Pend, Z.; Li, Z.; Yu, L.; Khor, K. A.; Xiong, Q., *Nano Energy*, **2015**, *15*, 688–696.